

# 1 **Titration of *in-cellula* affinities of protein-protein** 2 **interactions**

3  
4 David Cluet, Blandine Vergier, Nicolas-Pierre Levy, Lucie Dehau, Alexandre Thurman, Ikram  
5 Amri and Martin Spichty<sup>#</sup>

6  
7 Laboratoire de Biologie et de Modélisation de la Cellule, Ecole Normale Supérieure de Lyon,  
8 CNRS, Université Lyon 1, Université de Lyon; 46 allée d'Italie; 69364 Lyon cedex 07; France.

9  
10 <sup>#</sup>) corresponding author. New address: Laboratoire d'Innovation Moléculaire et Applications,  
11 Université de Strasbourg – Centre National de la Recherche Scientifique – Université de Haute-  
12 Alsace, 3 bis rue Alfred Werner, 68057 Mulhouse Cedex, France; Phone: +33 389 33 68 62;  
13 Email: martin.spichty@uha.fr.

14

15

16

17

18

19

20

21

22

23

24 **KEYWORDS:** protein-protein interactions, quantitative yeast-two hybrid, flow cytometry,  
25 single-cell analysis.

26

27 **A genetic assay permits simultaneous quantification of two interacting proteins and their**  
28 **bound fraction at the single-cell level using flow cytometry. *In-cellula* affinities of protein-**  
29 **protein interactions can be extracted from the acquired data through a titration-like**  
30 **analysis. The applicability of this approach is demonstrated on a diverse set of interactions**  
31 **with proteins from different families and organisms and with *in-vitro* dissociation**  
32 **constants ranging from picomolar to micromolar.**

33 The quest for methods that permit rapid and reliable determination of the affinity of  
34 protein-protein interactions (PPI) is unbroken. In contrast to biochemical *in-vitro* methods such  
35 as Isothermal Titration Calorimetry (ITC) and Surface Plasmon Resonance (SPR) that require  
36 purified proteins, quantitative genetic assays rely on the expression of the proteins of interest  
37 in cells. Many of these assays<sup>1-5</sup> are inspired by the yeast two-hybrid (Y2H) technique<sup>6</sup> which  
38 is based on the *in-cellula* expression of two proteins, usually named Bait and Prey, fused to an  
39 DNA-binding domain (BD) and an activation domain (AD), respectively. Upon physical  
40 interaction of the BD-Bait and AD-Prey proteins, a functional transcription factor is  
41 reconstituted that drives the expression of a reporter gene. The stronger the interaction, the  
42 higher should be the expression level of the reporter.<sup>7</sup> However, the expression level of the AD-  
43 Bait and BD-Prey play an important role, too.<sup>8</sup>

44 We recently introduced a quantitative yeast-two hybrid system (qY2H) that permits for  
45 the first time simultaneous quantification of BD-Bait, AD-Prey and the reporter at the single-  
46 cell level without the need of any antibodies or purified proteins.<sup>8</sup> Instead, we take advantage  
47 of fluorescent fusion proteins (Fig. 1A) that can be detected by standard flow cytometers. Here  
48 we show how this qY2H method can be exploited to perform *in-cellula* affinity titrations by  
49 applying the following two important improvements:

50 1) Cellular contents of fluorescent proteins are determined in units of Molecules of  
51 Equivalent Soluble Fluorochrome (MESF), so that measured quantities become independent of

52 the applied apparatus setup. It facilitates the future transferability of the qY2H measurements  
53 to other flow cytometers and allows researchers to consistently compare their results. Our  
54 reference fluorochrome is the yeast Enhanced Green Fluorescent protein (yEGFP) for which  
55 commercial calibration beads exist. The fluorescence intensity of TagRFP is converted into  
56 units of MESF of EGFP using independent calibration experiments with a fluorescent tandem  
57 protein BD-TagRFP-EGFP (see “Methods”).

58 2) We analyze the data by a titration-like procedure which allows the straightforward  
59 extraction of *in-cellula* dissociation constants for Bait:Prey interactions. In a proof of concept,  
60 we apply this *in-cellula* titration approach to a diverse set of PPIs with dissociation constants  
61 ranging from 117 pM to 17  $\mu$ M (Table 1). As in *in-vitro* SPR experiments, each PPI can be  
62 measured by Y2H in two different orientations (by exchanging Bait and Prey). Here we study  
63 only the orientation that produced the higher reporter level.<sup>8</sup> This orientation is considered as  
64 the molecular configuration with the higher accessibility of the PPI binding interface.<sup>7</sup>

65 In our qYH2 experiments, diploid yeast cells with constitutive expression of BD-Bait  
66 and induced expression of AD-Prey are cultured for two hours. Then, their fluorescence  
67 intensity is measured by flow cytometer in the three channels corresponding to TagRFP (BD-  
68 Bait), EGFP (AD-Prey), and TagBFP (reporter). Due to phenotypic variations, BD-Bait and  
69 AD-Prey are expressed at different levels among these cells which can be exploited to “prepare  
70 samples” for a titration. By gating, we can split the global heterogeneous ensemble of cells into  
71 several homogenous subensembles (bins). Each bin contains only cells within two specific,  
72 narrow intervals of red and green fluorescence intensity centered at values  $R$  and  $G$ ,  
73 respectively. Assuming a linear relationship between fluorescence intensity and molecule  
74 numbers,  $R$  and  $G$  can be considered as measures for the mean cellular content of BD-Bait and  
75 AD-Prey in the corresponding bin.

76 With the mean value of the blue fluorescence intensity, we can calculate for each bin

77 the normalized reporter level  $\varphi$ . It is obtained by forming the ratio of the expression level for  
78 the interaction of interest,  $E_{\text{interaction}}$  (Fig. 1A) and the level for a covalent BD-AD fusion,  
79  $E_{\text{covalent}}$  (Fig. 1B). This normalization renders  $\varphi$  dimensionless and independent of the  
80 acquisition apparatus (assuming again a linear relationship between molecule number and  
81 fluorescence intensity). Most importantly, we consider that  $\varphi$  reflects the time-averaged  
82 fraction of BD-Bait bound by AD-Prey during the reaction (as explained in the caption of Fig.  
83 1). Thus, titration curves can be obtained when  $\varphi$  is plotted as a function of  $G$  while keeping  $R$   
84 fixed (Fig. 1C). The curves can be fitted with the following Langmuir-type equation:

$$\varphi(G) \cong \beta \frac{G/\alpha}{K'_d + R + G/\alpha}$$

86 Eq. 1

87 where  $K'_d$  is the *in-cellula* dissociation constant (in units of MESF of EGFP) and  $\alpha$  and  $\beta$  are  
88 dimensionless parameters that empirically account for the fact that  $\varphi$  is a time-integrated  
89 property. The parameter  $\alpha$  reduces the final cellular content of AD-Prey (measured at the end  
90 of the reaction,  $G$ ) to the time-averaged content (over the entire reaction course,  $\langle G \rangle$ ). Since  
91 the induction kinetics under the GAL1-promotor in yeast<sup>9</sup> displays a quadratic-like time  
92 dependence (for short induction times), a reasonable choice for  $\alpha$  is  $3 [\langle G \rangle =_0 \int_0^1 G t^2 dt = G/3]$ .  
93 The prefactor  $\beta$ , on the other hand, integrates differences in the expression kinetics of the  
94 reporter for  $E_{\text{interaction}}$  (induced expression) and  $E_{\text{covalent}}$  (constitutive expression). It can be  
95 determined experimentally by monitoring  $\varphi$  for  $G \rightarrow \infty$  using a high-affinity couple (such as  
96 BD-Barstar29F/AD-BarnaseH102A).

97 We recommend that the titrations are carried out with the lowest possible value of  
98  $R=R_{\text{min}}$  (as defined by the detection limit of TagRFP by flow cytometry, see “Methods”). It  
99 limits overexpression and associated protein burden effects.<sup>10</sup> Furthermore, the auto-activation  
100 potential of the BD-Bait fusion is kept at a minimum, too.<sup>11</sup> Also, it mimics the condition of *in-*

101 *vitro* affinity titration experiments where the concentration of the titrated species (here BD-  
102 Bait) is kept fixed and as low as possible to avoid saturation effects. For the titrations with  
103  $R=R_{\min}$  the parameters  $\alpha=3$  and  $\beta=1.35$  were used to extract the  $K^2_d$ -values.

104 Despite substantial differences between our *in-cellula* system and *in-vitro* setups (as  
105 previously discussed<sup>8</sup> in detail), the *in-cellula* affinities strongly correlate with those from *in-*  
106 *vitro* measurements ( $R^2=0.91$ , Fig. 1D). The slope of the regression line is 0.84. Other *in-cellula*  
107 assays usually find lower correlation coefficients ( $< 0.9$ ) and significantly lower values for the  
108 slope of the regression line (0.2-0.6).<sup>1-5</sup> This is even more remarkable if one considers that the  
109 tested set of PPIs in this work is significantly more diverse. It may indicate a higher sensitivity  
110 for the qY2H titration approach; more testing will be necessary to confirm this surmise.

111 The presented protocol is robust as witnessed by the small error bars in the titration  
112 curves (Fig. 1c). All steps of the protocol have been optimized in liquid phase that can be easily  
113 automated for the use of microplates and integrated within robotic pipelines. It sets the stage  
114 for high-throughput affinity screenings of PPIs using cross-mating approaches<sup>12</sup> with libraries  
115 of yeast clones. As an outlook, affinity-based networks<sup>13</sup> can be created by attributing weights  
116 to the PPI edges according to their effective affinities. It contrasts standard Y2H screens that  
117 yield networks with only binary information (YES or NO). The topology of edge-weighted  
118 networks may help identifying key pathways within the network, and how they change as a  
119 function of environmental conditions (stress, metabolism, *etc*). Thus, we anticipate that high-  
120 throughput qY2H affinity data would boost the modelling of interactomes and thereby advance  
121 significantly systems biology.

## 122 **Methods**

123 The qY2H experiments, acquisitions by flow cytometry and analyses were carried out  
124 as described in our previous study<sup>8</sup> with the following particularities. About  $10^7$  cells were  
125 cultured per experiment and interaction (including the covalent BD-AD fusion and the control

126 sample BD-Empty / AD-Empty). To ensure that these cells have been indeed transfected with  
127 all three vectors, we selected for the analysis large (=growing) cells with a forward scatter range  
128  $75\ 000 < \text{FSC-H} < 125\ 000$ ; “H” indicates signal height. Furthermore, only cells with a red  
129 fluorescence intensity of  $800 \pm 100$  TagRFP-H were analysed. This bin is located just above  
130 the 95% threshold of the non-fluorescent cells,<sup>8</sup> and therefore defines  $R_{\min}$ .

131 The mean Tag BFP-H value was then calculated for bins of varying  $G$  values from -500  
132 to 25500 yEGFP-H (bin size 1000). For each bin we calculated:

$$133 \quad \varphi(G) = \frac{\langle F_{\text{BFP,interaction}} \rangle_G - \langle F_{\text{BFP,CTRL}} \rangle_G}{\langle F_{\text{BFP,covalent}} \rangle_G - \langle F_{\text{BFP,CTRL}} \rangle_G}$$

134 Eq. 2

135 where  $\langle F_{\text{BFP,X}} \rangle_G$  is the mean blue fluorescence intensity. The subscripted X refers to the  
136 physical interaction, covalent fusion or control couple. The control couple BD-Empty / AD-  
137 Empty<sup>8</sup> permits to remove the background of the reporter system.

138 Finally,  $G$  values were converted into MESF of EGFP using calibration beads (Ozyme,  
139 reference 632594) following the manufacturer’s protocol. For the conversion of  $R_{\min}$ , we  
140 performed independent calibration measurements with diploid yeast cells expressing the  
141 fluorescent tandem fusion protein BD-TagRFP-yEGFP (under the same condition as the qY2H  
142 experiments). Cells with a red fluorescence intensity of  $800 \pm 100$  TagRFP-H displayed a mean  
143 green fluorescence intensity of 370 000 MESF of EGFP (=  $R_{\min}$  used in Eq. 1).

144 Experiments and analyses were performed at least three times for each interaction and  
145 averaged titration curves were least-square fitted with Eq. 1.

146 ..

147

148

149 **Figures & Tables**

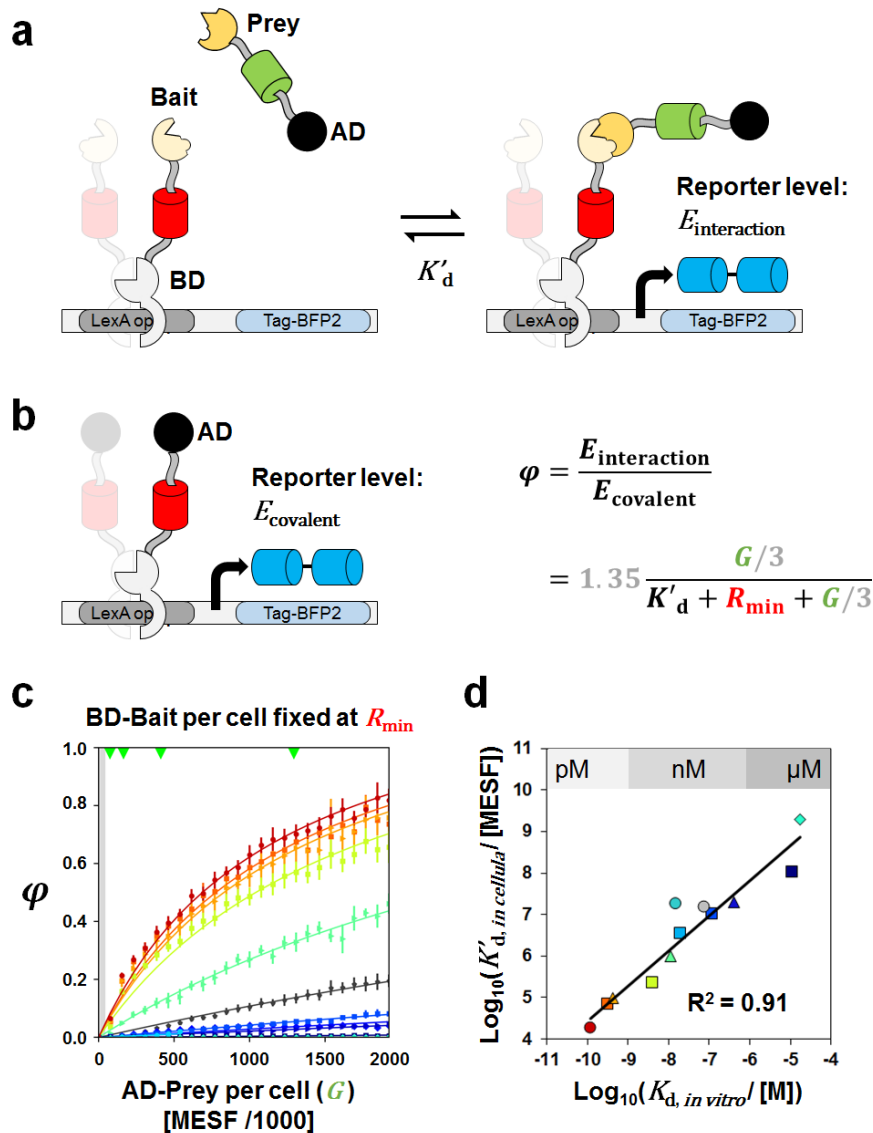
150 **Table 1: Investigated protein-protein interactions and their *in-vitro* affinities ( $K_d$ ).**

Bait proteins					Prey proteins						
Organism	Family	Name	Mutant	MW	$K_d$ (nM)	Symbol	Organism	Family	Name	Mutant	MW
<i>B. amylo-liquefaciens</i>	RNase inhibitor	Barstar	WT	10	320 <sup>a</sup>	■	<i>B. amylo-liquefaciens</i>	RNase	Barnase	H102A	12
			Y29A	10	420 <sup>a</sup>	▲					
			Y29F	10	117 <sup>a</sup>	●					
			W38F	10	4 000 <sup>a</sup>	■					
			D35A	10	25 000 <sup>h</sup>	○					
			D39A	10	420 000 <sup>b</sup>	▲					
<i>H. sapiens</i>	GTPase	HRas	G12V & C186A	21	122 000 <sup>c</sup>	■	<i>H. sapiens</i>	Kinase	CRaf RBD	WT	9
					11 000 <sup>d</sup>	▲				A85K	9
<i>H. sapiens</i>	Kinase regulatory subunit	CksHs1	WT	10	77 000 <sup>e</sup>	■	<i>H. sapiens</i>	Kinase	CDK2	WT	34
<i>E. coli</i>	$\beta$ -Lactamase	TEM	WT	31	15 000 <sup>f</sup>	●	<i>S. clavuligerus</i>	$\beta$ -Lactamase inhibitor	BLIP1	WT	21
<i>HIV1</i>	Virulence factor	Nef	LAI	23	11 400 000 <sup>g</sup>	■	<i>H. sapiens</i>	Kinase	SRC SH3	WT	7
<i>H. sapiens</i>	Adapter	Grb2 SH3	WT	7	17 000 000 <sup>i</sup>	◆	<i>M. musculus</i>	Nucleotide exchange factor	Vav1 SH3	WT	8

151 <sup>a</sup> ITC, 50mM Tris/HCl, pH 8 at 25°C.<sup>14</sup>  
 152 <sup>b</sup> Mean values from two studies<sup>14,15</sup> with ITC, 24mM Hepes, pH 8, 1 mM DTT at 25°C.  
 153 <sup>c</sup> Mean values from four studies of Ras G12V (without the membrane anchor): SPR, 50 mM Tris/HCl, pH 7.4, 100mM NaCl, 5 mM  
 154 MgCl<sub>2</sub>;<sup>16</sup> SPR, 50 mM Tris/HCl, pH 7.4, 100mM NaCl, 5 mM MgCl<sub>2</sub>;<sup>17</sup> SPR, 10 mM Hepes, pH 7.4, 150 mM NaCl, 2 mM MgCl<sub>2</sub>, and  
 155 0.01% Nonidet P-40 25°C;<sup>18</sup> ITC, 50 mM Hepes, pH 7.4, 125 mM NaCl, 5 mM MgCl<sub>2</sub>, 25°C.<sup>19</sup>  
 156 <sup>d</sup> ITC, 50 mM Hepes, pH 7.4, 125 mM NaCl, 5 mM MgCl<sub>2</sub>, 25°C.<sup>19</sup> The dissociation constant of the CRaf RBD A85K mutant was measured  
 157 with HRas WT loaded with a GTP-analogue. The mutant HRas G12V is known to decrease the dissociation constant for the interaction with  
 158 CRaf RBD WT by a factor of 11.<sup>20</sup> The given value applies the same correction factor.  
 159 <sup>e</sup> SPR, 10 mM Hepes, 3.4 mM EDTA, 150 mM NaCl, 0.001% surfactant P20, pH 7.4.<sup>21</sup>  
 160 <sup>f</sup> SPR, 10 mM Hepes, 3.4 mM EDTA, 150 mM NaCl, 0.05% surfactant P20, pH 7.4.<sup>22</sup>  
 161 <sup>g</sup> ITC, 20 mM phosphate buffer, pH 7.5, 150 mM NaCl, 2 mM EGTA, and 5 mM DTT, 25°C.<sup>23</sup>  
 162 <sup>h</sup> SPR, 10 mM Hepes-Na, pH 7.4, 0.15 M NaCl, 3 mM EDTA, and 0.005% (v/v) Tween 20, 25 °C.<sup>24</sup>  
 163 <sup>i</sup> SPR, 25°C.<sup>25</sup>  
 164 <sup>h</sup> Free-energy calculations.<sup>8</sup>  
 165

166

167 **Figure 1.**



168  
169  
170  
171  
172  
173  
174  
175  
176  
177  
178  
179  
180  
181  
182  
183  
184  
185  
186  
187

**a**) In our qY2H system, red-fluorescent BD-Bait interacts with green-fluorescent AD-Prey to reconstitute a transcription factor that drives the expression of a blue-fluorescent reporter. Our hypothesis is that the expression level of the reporter,  $E_{\text{interacting}}$ , reflects the number of BD-molecules bound to the promoter corrected by the fraction of BD-Bait bound to AD-Prey. This fraction is influenced by the affinity between the Bait and the Prey, but also by the expression levels of BD-Bait and AD-Prey. **b**) When the activation domain is covalently linked to the DNA-binding domain, the expression level  $E_{\text{covalent}}$  depends only on the number of BD-Bait molecules bound to the promoter. Thus, when forming the quantity  $\varphi$  by dividing  $E_{\text{interacting}}$  with  $E_{\text{covalent}}$ , we obtain a measure for the fraction of BD-molecules bound by an AD-Prey molecule. To determine  $E_{\text{covalent}}$ , we constructed a BD-AD fusion protein. Unfortunately, the activation domain B42 (as used in **a**) turned out to be toxic for our yeast strains when used in the BD-AD construct. Instead, we used the activation domain B112. Difference in the activation potential between B42 and B112 are integrated in the parameter  $\beta$  of Eq. 1. **c**) The quantity  $\varphi$  can be monitored as a function of different levels of EGFP Molecules of Equivalent Soluble Fluorochrome (MESF) corresponding to different cellular levels of AD-Prey. In these titrations, the level of BD-Bait is kept fixed at the lowest possible value (see “Methods”). For the interaction TEM/BLIP1 (cyan line) the titration can be performed only up to one third of the titrant quantity due to expression problems of AD-BLIP1.<sup>8</sup> Green triangles at the top vertical axis indicate the position of used calibration beads. **d**) When the titration curves are fitted with Eq. 1, we can extract the dissociation constant in units of MESF ( $K'_d$ ). The estimated  $K'_d$ -values show a remarkable correlation with the dissociation constants measured from alternative *in-vitro* experiments (Table 1).



188 References

- 189 1. Dutta, S., Koide, A. & Koide, S. High-throughput Analysis of the Protein Sequence–  
190 Stability Landscape using a Quantitative Yeast Surface Two-hybrid System and Fragment  
191 Reconstitution. *J. Mol. Biol.* **382**, 721–733 (2008).
- 192 2. Jeong, K. J., Seo, M. J., Iverson, B. L. & Georgiou, G. APEx 2-hybrid, a quantitative  
193 protein-protein interaction assay for antibody discovery and engineering. *Proc. Natl.*  
194 *Acad. Sci.* **104**, 8247–8252 (2007).
- 195 3. Colas, P., Cohen, B., Ferrigno, P. K., Silver, P. A. & Brent, R. Targeted modification and  
196 transportation of cellular proteins. *Proc Natl Acad Sci USA* **97**, 13720–13725 (2000).
- 197 4. Hu, X., Kang, S., Chen, X., Shoemaker, C. B. & Jin, M. M. Yeast Surface Two-hybrid for  
198 Quantitative *in Vivo* Detection of Protein-Protein Interactions via the Secretory Pathway.  
199 *J. Biol. Chem.* **284**, 16369–16376 (2009).
- 200 5. Younger, D., Berger, S., Baker, D. & Klavins, E. High-throughput characterization of  
201 protein–protein interactions by reprogramming yeast mating. *Proc. Natl. Acad. Sci.* **114**,  
202 12166–12171 (2017).
- 203 6. Fields, S. & Song, O. A novel genetic system to detect protein protein interactions.  
204 *Nature* **340**, 245–246 (1989).
- 205 7. Estojak, J., Brent, R. & Golemis, E. A. Correlation of two-hybrid affinity data with *in*  
206 *vitro* measurements. *Mol. Cell. Biol.* **15**, 5820–5829 (1995).
- 207 8. Cluet, D. *et al.* A quantitative tri-fluorescent yeast two-hybrid system: from flow  
208 cytometry to *in-cellula* affinities. *Mol. Cell. Proteomics* (2020)  
209 doi:10.1074/mcp.TIR119.001692.
- 210 9. Li, J. *et al.* Green fluorescent protein in *Saccharomyces cerevisiae*: Real-time studies of  
211 the GAL1 promoter. *Biotechnol. Bioeng.* **70**, 187–196 (2000).
- 212 10. Bolognesi, B. & Lehner, B. Reaching the limit. *eLife* **7**,.

- 213 11. Rajagopala, S. V. & Uetz, P. Analysis of Protein–Protein Interactions Using High-  
214 Throughput Yeast Two-Hybrid Screens. in *Network Biology* (eds. Cagney, G. & Emili,  
215 A.) vol. 781 1–29 (Humana Press, 2011).
- 216 12. Kolonin, M. G., Zhong, J. & Finley, R. L. Interaction mating methods in two-hybrid  
217 systems. *Methods Enzymol.* **328**, 26–46 (2000).
- 218 13. Gromiha, K. Y. and M. M. Analysis of protein-protein interaction networks based on  
219 binding affinity. *Current Protein & Peptide Science*  
220 <http://www.eurekaselect.com/135165/article> (2016).
- 221 14. Schreiber, G. & Fersht, A. R. Energetics of protein-protein interactions: Analysis of the  
222 Barnase-Barstar interface by single mutations and double mutant cycles. *J. Mol. Biol.*  
223 **248**, 478–486 (1995).
- 224 15. Frisch, C., Schreiber, G., Johnson, C. M. & Fersht, A. R. Thermodynamics of the  
225 interaction of barnase and barstar: changes in free energy versus changes in enthalpy on  
226 mutation 1 1 Edited by J. Karn. *J. Mol. Biol.* **267**, 696–706 (1997).
- 227 16. Herrmann, C., Horn, G., Spaargaren, M. & Wittinghofer, A. Differential Interaction of the  
228 Ras Family GTP-binding Proteins H-Ras, Rap1A, and R-Ras with the Putative Effector  
229 Molecules Raf Kinase and Ral-Guanine Nucleotide Exchange Factor. *J. Biol. Chem.* **271**,  
230 6794–6800 (1996).
- 231 17. Block, C., Janknecht, R., Herrmann, C., Nassar, N. & Wittinghofer, A. Quantitative  
232 structure-activity analysis correlating Ras/Raf interaction in vitro to Raf activation in  
233 vivo. *Nat. Struct. Mol. Biol.* **3**, 244–251 (1996).
- 234 18. Fischer, A. *et al.* B- and C-RAF display essential differences in their binding to Ras: the  
235 isotype-specific N terminus of B-RAF facilitates Ras binding. *J. Biol. Chem.* **282**, 26503–  
236 26516 (2007).

- 237 19. Kiel, C. *et al.* Improved Binding of Raf to Ras·GDP Is Correlated with Biological  
238 Activity. *J. Biol. Chem.* **284**, 31893–31902 (2009).
- 239 20. Kiel, C. Untersuchung von Ras/Effektor-Komplexen mit gezielt veränderten  
240 elektrostatischen Eigenschaften. (Dissertation, Ruhr-Universität Bochum, Fachbereich  
241 Biochemie, 2003).
- 242 21. Bourne, Y. *et al.* Crystal Structure and Mutational Analysis of the Human CDK2 Kinase  
243 Complex with Cell Cycle–Regulatory Protein CksHs1. *Cell* **84**, 863–874 (1996).
- 244 22. Albeck, S. & Schreiber, G. Biophysical Characterization of the Interaction of the  $\beta$ -  
245 Lactamase TEM-1 with Its Protein Inhibitor BLIP<sup>†</sup>. *Biochemistry (Mosc.)* **38**, 11–21  
246 (1999).
- 247 23. Arold, S. *et al.* RT Loop Flexibility Enhances the Specificity of Src Family SH3 Domains  
248 for HIV-1 Nef<sup>†, ‡</sup>. *Biochemistry (Mosc.)* **37**, 14683–14691 (1998).
- 249 24. Sato, Y. *et al.* Characterization of the Interaction between Recombinant Human Peroxin  
250 Pex3p and Pex19p: *IDENTIFICATION OF TRP-104 IN Pex3p AS A CRITICAL*  
251 *RESIDUE FOR THE INTERACTION.* *J. Biol. Chem.* **283**, 6136–6144 (2008).
- 252 25. Nishida, M. Novel recognition mode between Vav and Grb2 SH3 domains. *EMBO J.* **20**,  
253 2995–3007 (2001).

254